https://doi.org/10.1007/s11467-023-1304-4

RESEARCH ARTICLE

Room-temperature vertical ferroelectricity in rhenium diselenide induced by interlayer sliding

Fang Li,[1] Jun Fu,[2] Mingzhu Xue,[3] You Li,[1] Hualing Zeng,[2] Erjun Kan,[1] Ting Hu,[1,†] Yi Wan[1, 3, ‡]

[1] MIIT Key Laboratory of Semiconductor Microstructure and Quantum Sensing, and Department of Applied Physics, Nanjing University of Science and Technology, Nanjing 210094, China
[2] International Center for Quantum Design of Functional Materials (ICQD), Hefei National Laboratory for Physical Sciences at the Microscale, and Department of Physics, University of Science and Technology of China, Hefei 230026, China
[3] State Key Laboratory for Artificial Microstructure & Mesoscopic Physics, School of Physics, Peking University, Beijing 100871, China
Corresponding authors. E-mail: †thu@njust.edu.cn, ‡wany@njust.edu.cn
Received March 30, 2023; accepted May 4, 2023

Supporting Information

The PDF file includes:

Section S1 CVT growth

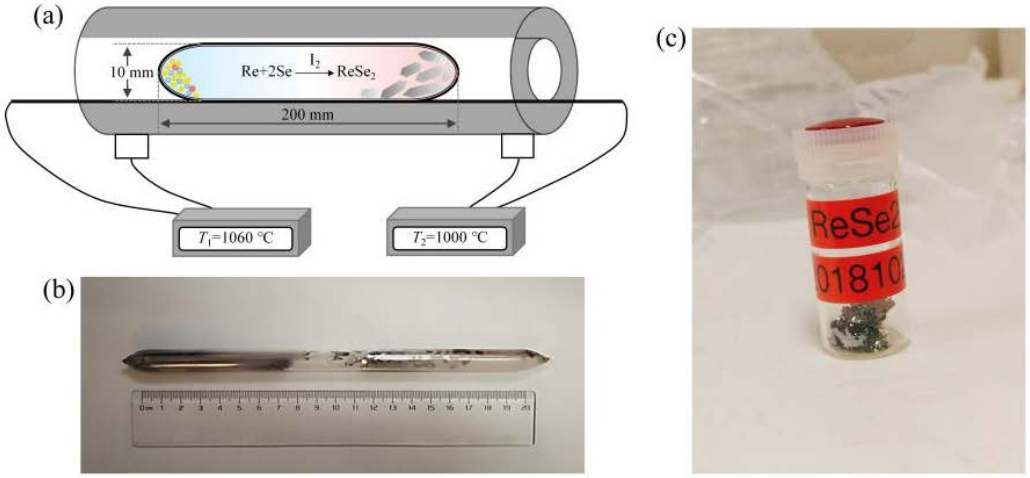

Fig. S1 **(a)** Schematic diagram of the CVT process for the preparation of $ReSe_2$ crystals. **(b)** The sealed ampoule (length: 200 mm; outer diameter: 10 mm) after CVT growth. **(c)** The CVT-synthesized $ReSe_2$ bulks.

CVT technique was utilized to synthesize the $ReSe_2$ bulk crystals based on the previous reports with slight modification[S1]. Rhenium powder (~22 mesh, 99.999%, Alfa Aesar) and selenium powder (~200 mesh, 99.99%, Aladdin) were used as received without further purification. Elements of Re and Se in stoichiometric proportion 1:2 were mixed as precursors to a total mass of around 500 mg to synthesize the $ReSe_2$ bulk. In addition to the elemental constituents, halogen (I_2, ~10 mg/cc) was employed as the transport agent in the synthetic process (Fig. S1, a). The mixed powders were sealed in an evacuated quartz ampule of 200 mm in length and 10 mm in outer diameter (Fig. S1, b), which was designed to enlarge the temperature gradient, with an internal pressure of 10^{-4} torr.

Initially, the source zone (T_1) and the growth zone (T_2) were gradually increased and kept at 900 and 1000℃, respectively, for 24 h. The pre-reaction process allows the constituents to completely react and prevents back transport. After that, the temperature of the source zone (T_1) was gradually increased to 1060℃, while that of the growth zone (T_2) remained at 1000℃. The growth process was kept for 72 h. Then, the temperatures of both zones were lowered to room temperature naturally. After the ampoule was taken out of the tube furnace, the well-grown compounds were collected for further characterizations and subsequent measurements (Fig. S1, c).

Section S2 XRD patterns of $ReSe_2$

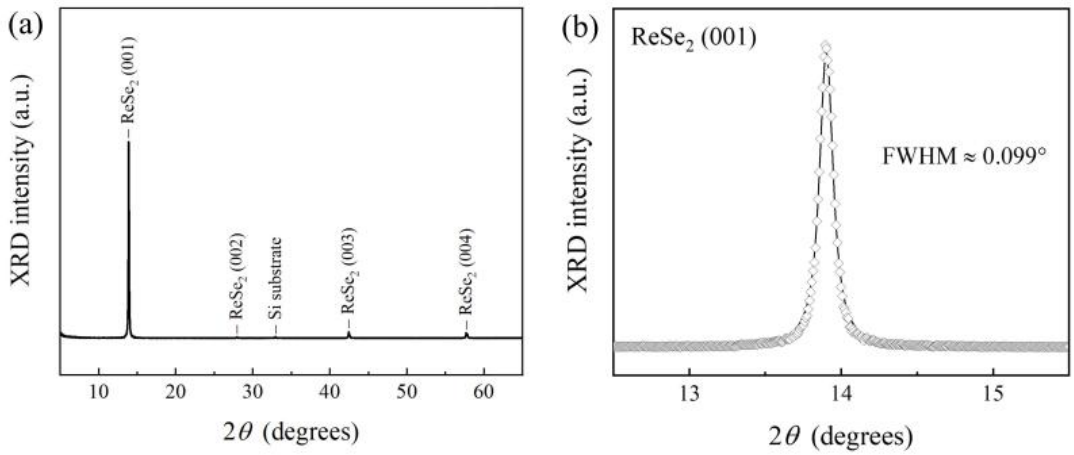

Fig. S2 (a) XRD pattern of $ReSe_2$ bulk crystals prepared by the CVT method. **(b)** Zoom-in XRD pattern corresponding to the (001) crystallographic plane of $ReSe_2$.

The crystallographic structure of $ReSe_2$ was examined by X-ray diffraction (XRD) (X' Pert Pro, PANalytical B.V.). To examine the crystal structures of the CVT-grown $ReSe_2$ samples, XRD pattern investigations were performed. As shown in Fig. S2, a, the reflection peaks located at around 13.9°, 28.0°, 42.5°, 57.7°, corresponding to the crystallographic planes of (001), (002), (003), (004), respectively, indicate the presence of triclinic $ReSe_2$. These patterns are consistent with the reference XRD patterns in the JCPDS card (Nos. 50-0537, 82-1379 and 89-0340) for pure triclinic $ReSe_2$[S2]. The strongest intensity of the (001) peak indicates the preferred orientation effect of the layered $ReSe_2$ crystal. The small full width at half maximum (FWHM) for (001) plane of around 0.099° (Fig. S2, b) indicates the superior crystallization quality.

Section S3 Raman spectra of $ReSe_2$

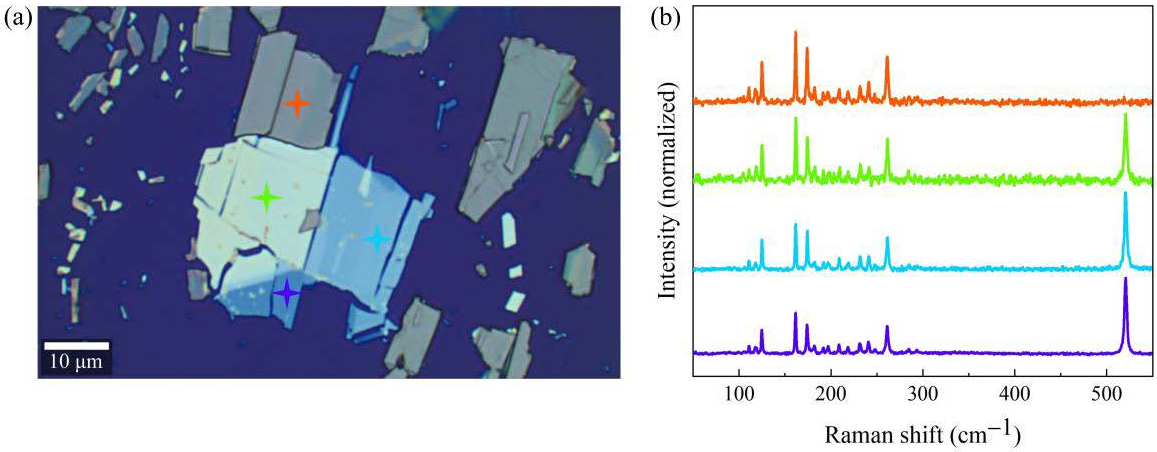

Fig. S3.1 (a) Optical microscopy image of mechanically exfoliated $ReSe_2$ samples supported atop SiO_2/Si wafer. **(b)** Non-polarized Raman spectra obtained from $ReSe_2$ flakes. The raw spectra were collected from the few-layer $ReSe_2$ regions as marked by cross stars with the same color in (a) and vertically offset for clarity.

The common Raman spectra without polarization information for $ReSe_2$ samples of various thicknesses (Fig. S3.1, a) are shown in Fig. S3.1, b. The densely spaced Raman modes of $ReSe_2$ have a frequency range of 100 to 300 cm^{-1}. And the silicon substrate is responsible for the peak at 520.7 cm^{-1}, which was detected as a result of light passing through the sample.

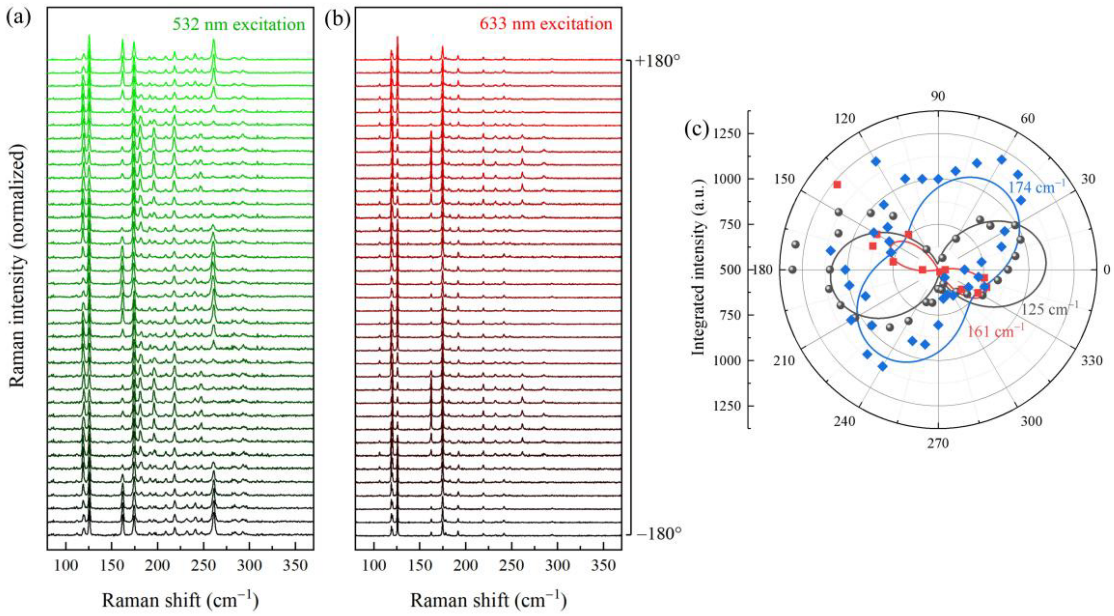

Fig. S3.2 Angular dependence of the Raman spectra of a few-layer $ReSe_2$ sample recorded as a function of the angle between the linear laser field and the Re chains at the excitation laser wavelength of 532 nm **(a)** and 633 nm **(b)**, under the parallel configuration. The raw spectra are normalized and vertically offset for clarity. **(c)** The dependence of Raman intensity on the polarization of the incident laser beam for three typical peaks located at around 125 cm^{-1} (gray), 161 cm^{-1} (red), and 174 cm^{-1} (blue). The three curves in the respective colors are fits from the Raman tensor analysis, and the symbols reflect experimental data for the integrated intensities of the three typical peaks. The excitation laser wavelength is 532 nm.

Figure S3.2 displays the angular dependence of the Raman response in $ReSe_2$, recorded as a function of the angle θ between the linearly polarized laser electric field and the Re chains at the excitation wavelength of 532 nm (Fig. S3.2, a) and 633 nm (Fig. S3.2, b)[S3, S4]. The Raman characteristic peaks of $ReSe_2$ display a clear variation of intensity with the angle for all modes, as an indication of in-plane anisotropy. The polar plots of the peak intensity as a function of the polarization angle make obvious the extent to which the peak intensities of Raman modes vary. The plots for three typical peaks at 125, 161, and 174 cm^{-1} are displayed in Fig. S3.2, c. The complicated lattice vibrations of $ReSe_2$[S5] make it challenging to match each Raman peak with a pure E_g or A_g mode, distinct from MoS_2[S6]. Consequently, according to their dominant vibration directions, we could identify these modes as E_g-like or A_g-like modes. The vibration of the 125 cm^{-1} mode is primarily in-plane and symmetric, making it an E_g-like mode. Since the primary vibrations are in the one-dimensional vertical direction, the 161 and 174 cm^{-1} peaks are A_g-like modes.

Section S4 Ferroelectric transition temperature for 2L $ReSe_2$

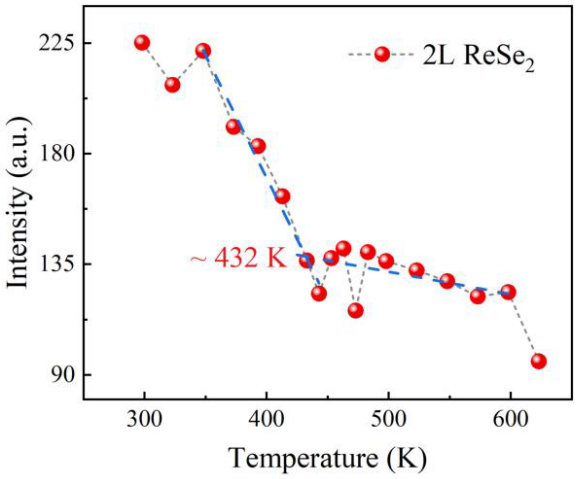

Fig. S4 Temperature-dependent SHG intensity for 2L $ReSe_2$.

2D ferroelectricity offers a platform for developing high-density memories and efficient information processing devices with low-energy consumption. Before shedding light on the device application potential, there is a need to examine the thermal stability of the vertical ferroelectricity in 1T'-$ReSe_2$, which is of great importance to evaluate the functionality of ferroelectrics. Here, we measured the ferroelectric transition temperature (T_C) of 2L 1T'-$ReSe_2$ by temperature-dependent SHG measurements. As shown in Figure S4, distinct SHG signals of 2L 1T'-$ReSe_2$ are observed at room temperature, while the SHG intensity decreases gradually with the increasing temperature and almost vanishes at higher temperature above 450 K. Based on a simple fitting, we estimate the T_C of 2L 1T'-$ReSe_2$ to be ~432 K. The high T_C endows semiconducting 1T'-$ReSe_2$ a promising candidate for the field of sliding ferroelectricity towards realistic applications.

Section S5 Comparison of the ferroelectric properties of $ReSe_2$ and ReS_2

Table S1 Comparison of the ferroelectric properties of $ReSe_2$ and ReS_2.

Material	Coercivity (V)	PFM amplitude (pm)	Transition temperature (K)	Reference
2L $ReSe_2$	1.6	70	432	This work
2L ReS_2	1.8	165	405	*Phys. Rev. Lett.*, 2022, 128(6): 067601

We make a comparison of the ferroelectric properties of $ReSe_2$ and ReS_2, including coercivity, PFM amplitude (which is proportional to the polarization intensity within a certain range), and ferroelectric transition temperature. As shown in Table S1, 2L $ReSe_2$ exhibits lower coercivity and polarization intensity while having a higher transition temperature than those of 2L ReS_2.

References

[S1] Z. Lai, A. Chaturvedi, Y. Wang, et al. Preparation of 1T'-phase $ReS_{2x}Se_{2(1-x)}$(x=0-1) nanodots for highly efficient electrocatalytic hydrogen evolution reaction, *J. Am. Chem. Soc.* 140(27), 8563 (2018)

[S2] L. Xing, X. Yan, J. Zheng, et al. Highly crystalline $ReSe_2$ atomic layers synthesized by chemical vapor transport, *InfoMat* 1(4), 552 (2019)

[S3] D. A. Chenet, B. Aslan, P. Y. Huang, et al. In-plane anisotropy in mono-and few-layer ReS_2 probed by Raman spectroscopy and scanning transmission electron microscopy, *Nano Lett.* 15(9), 5667 (2015)

[S4] E. Lorchat, G. Froehlicher, and S. Berciaud, Splitting of interlayer shear modes and photon energy dependent anisotropic Raman response in N-layer $ReSe_2$ and ReS_2, *ACS Nano* 10(2), 2752 (2016)

[S5] H. Zhao, J. Wu, H. Zhong, et al. Interlayer interactions in anisotropic atomically thin rhenium diselenide, *Nano Res.* 8, 3651 (2015)

[S6] S. L. Li, H. Miyazaki, H. Song, et al. Quantitative Raman spectrum and reliable thickness identification for atomic layers on insulating substrates, *ACS Nano* 6(8), 7381 (2012)